Adsorption (2024) 30:95–106
https://doi.org/10.1007/s10450-023-00433-8

^{2}H-NMR study of molecular reorientation of D_2O confined into the slit-shaped micropores of activated carbon fiber

Takumi Asada[1] · Rin Iwatsuki[2] · Taku Iiyama[2] · Takahiro Ueda[1]

Received: 11 August 2023 / Revised: 17 November 2023 / Accepted: 21 November 2023 / Published online: 5 January 2024

Abstract
Herein, the reorientation of heavy water (D_2O) molecules adsorbed in the slit-type micropores of activated carbon fibers is investigated using the ^{2}H-nuclear magnetic resonance technique. The rotational correlation times (τ_c) of D_2O are evaluated from the ^{2}H spin–lattice relaxation time (T_1). The obtained τ_c values are significantly influenced by both the pore-filling ratio (ϕ) and temperature, thus suggesting that the adsorption of D_2O into activated carbon fibers (ACF) effectively influences the reorientation of the D_2O molecules within the ACF. The reorientational motion of D_2O is examined by the extended jump model. According to this model, the nanoconfinement effect, which results from the reduction in free volume around D_2O, is attributed to the transition-state excluded volume effect, whereas the effect of hydrogen bonding between the D_2O and surface functional groups is attributed to the transition-state hydrogen bonding effects. Furthermore, the dependence of τ_c on ϕ is explained by the chemical exchange between the pore surface adsorption sites and the central space of the pore. Thus, the dynamic behavior of adsorbed D_2O molecules reveals the mechanism of D_2O adsorption into the ACF micropores.

Keywords Water adsorption · NMR · Spin–lattice relaxation time · Reorientation · Micropore filling · Hydrogen bond

1 Introduction

Water is essential for life, in large part owing to its several unique properties that are different from those of other liquids. In particular, the density of water reaches the maximum value at 4 °C. Freezing of water decreases its density, resulting in the shift of the solid–liquid equilibrium curve in the phase diagram to lower temperatures with increasing pressure. The phase diagram of water is complex and comprises multiple structures [1–3], with several phases discovered in the last several years. For example, Yamane et al. revealed the ice XIX phase using dielectric measurements and neutron powder diffraction [4], whereas Gasser et al. [5] identified a new ice polymorph that differs from ice XV and ice VI and a second hydrogen-ordered polymorph of ice VI using high-resolution neutron powder diffraction. The ice VII phase is considered as "superionic conducting ice," in which protons diffuse rapidly through a solid oxygen lattice at high pressures and temperatures [6]. Following the discovery of ice VII in deep planetary layers, the existence of this phase was experimentally verified through laser-driven shock compression. Thus, the structure and properties of water and ice are not fully understood and require extensive further research [7, 8].

The unique properties of water are particularly important in constrained nanoscale spaces. Nanospaces can be categorized based on their dimensionality into "1D," "2D," and "3D" spaces. The phase diagrams of water and ice in 1D and 2D nanospaces have been reported by several research groups [9, 10]. The arrangement of water molecules in carbon nanotubes is considerably affected by the pore size, and a phase diagram representing the relationships between the water structure and carbon nanotube pore size was constructed [10]. Water sandwiched by monolayer graphene sheets has been studied using molecular simulations, and the phase diagram for water in 2D nanospace has been reported [9]. Monolayer water has diverse phases, with different molecular phases showing pressure-dependent melting points. Monolayer water is found in a hexatic phase, which is a unique liquid crystal phase in a 2D space. Additionally, a superionic conducting phase with high electrical

✉ Takahiro Ueda
ueda@chem.sci.osaka-u.ac.jp

[1] Department of Chemistry, Graduate School of Science, Osaka University, Toyonaka, Osaka 560-0043, Japan

[2] Department of Chemistry, Faculty of Science, Shinshu University, Matsumoto, Nagano 390-8621, Japan

conductivity has been predicted. Thus, water and ice exhibit different behaviors in 1D and 2D nanospaces from that in 3D bulk space. Therefore, the exploitation of nanoconfinement effects may be a promising approach for accessing novel and unique properties of water and ice.

Unique structures and properties, such as negative dielectric constant [11] and fast proton transfer, that differ from those of bulk water have been found in sub-nanometer-sized spaces [12]. These unique properties arise from the strong adsorption potential of the pore walls and the spatial constraints that affect the water structure. The behavior of water in carbon-based hydrophobic micropores is of particular interest because of its importance for filtration and separation technologies [13]. Activated carbon fibers (ACF) are important and widely available porous carbon materials, and their pore structure has been characterized as pseudo-2D slit-shaped sub-nanometer spaces [14, 15]. Kaneko et al. conducted numerous pioneering studies on water adsorption in the hydrophobic nanospace of ACF with a pseudo-2D structure. Based on a detailed study on water adsorption, they proposed that the adsorption mechanism of water into ACF consists of the formation of water clusters, followed first by cluster growth and then by their coalescence within a pore [16–18].

The adsorption of water in the ACF micropores depends on the temperature as well as the amounts and types of the surface functional groups. Horikawa et al. [19] determined the temperature dependence of water cluster growth via molecular dynamic simulations. Liu et al. [20] conducted a comprehensive Monte Carlo simulation study on water adsorption in a functionalized graphitic slit pore for different types of surface functional groups (acidic and basic) and their configurations. Furthermore, Ito et al. [21, 22] studied the kinetics of the water cluster-mediated micropore filling, they found that the rate constants depend on the pore size and the rate-determining steps are associated with the formation of water molecular assemblies. Recent developments and studies on water adsorption on carbons were reviewed by Liu et al. [23].

Water in ACF with slit-shaped nanopores exhibits unique behavior that is different from that of bulk water. Futamura et al. [24] examined water density changes in ACF with a slit width of 1.36 nm using X-ray diffraction (XRD) measurements at temperatures ranging from 30 K to room temperature [24, 25]. They found that water has an ice-like structure below 200 K, whereas its density increases rapidly above 200 K and becomes equivalent to that of a liquid at 280 K. Essentially, the density changes smoothly from that of ice to that of water without any evident phase transitions. Recently, Sugiyama et al. [26] reported that ice-like structures can be maintained in sub-nanometer spaces with slit widths of less than 1 nm even at higher temperatures. This behavior is observed only in spaces smaller than 1 nm. Water also forms a 2D ice-like structure in the nanopores of 2D graphene [27]. In addition, pore wall properties, including hydrophobicity, hydrophilicity, surface functional groups, and pore-filling ratio, affect the behavior of water in sub-nanometer spaces.

In our previous study, we have examined the molecular motion of water saturated in ACF nanopores with slit widths of 1.1 and 0.7 nm [28]. Evidently, tetrahedral jumps of water molecules similar to those in bulk ice were dominant for the slit width of 1.1 nm, whereas 180° flipping dominated at the slit width of 0.7 nm. Spatial constraints in pseudo-2D structures considerably affect the behavior of water at the sub-nanometer scale. ^{2}H-nuclear magnetic resonance (NMR) lines typical of liquids were observed above 200 K, indicating that water in the micropores behaved as a liquid. This result is consistent with the findings of Futamura et al. [24]. However, to the best of our knowledge, with the exception of our previous work, experimental studies on the molecular motion of water adsorbed in the ACF micropores are limited. Understanding the relationship between water-cluster formation and molecular motion can reveal unique properties of water in small hydrophobic spaces. Additionally, studies on dynamic behavior can reveal the unique structure of water in sub-nanospaces, as reported by Sugiyama et al. [26].

Recently, Wang et al. [29] characterized the porosity of nanoporous carbon using water adsorption by monitoring the amount of adsorbed water via in-situ NMR. Furthermore, Song et al. used in-site NMR to reveal the nucleation and growth process of water adsorption in the micropores of activated carbons [30]. They examined the nucleus-independent chemical shift (NICS) of the water adsorbed in activated carbon as a function of the relative pressure of water vapor, reporting direct experimental evidence of the nucleation and growth processes of water inside activated carbon micropores.

NMR can detect molecular motion in water molecules through the signals of the ^{1}H, ^{2}H, and ^{17}O nuclei by selecting the appropriate probe nucleus [31]. The T_1 value of the ^{2}H nuclei is linked to the rotational correlation time (τ_c) of water molecules. For the ^{2}H nuclei, the T_1 spin–lattice relaxation time can elucidate the molecular rotation of heavy water (D_2O) with a correlation time of the order of ps [32]. In this study, we examined the dependence of the ^{2}H T_1 of D_2O adsorbed in the hydrophobic slit-shaped sub-nanometer-sized spaces of ACF on the pore-filling ratio. First, we measured water adsorption isotherm on ACF in order to evaluate the pore-filling ratio of D_2O. Subsequently, we observed ^{2}H spin–lattice relaxation time as well as the broad-band spectrum for D_2O confined in ACF. The correlation time of D_2O reorientation was analyzed using the extended jump model (EJM) [33, 34]. Furthermore, we examined the intermolecular interactions involved in the formation of water clusters by evaluating the activation energy for the reorientation of D_2O as determined by the temperature dependence of ^{2}H T_1

values. Based on the analysis of molecular motion we discussed the strong hydrogen bond formation between surface functional groups and D_2O as well as water-cluster formation in ACF pores.

2 Experimental

2.1 Materials

The ACF used herein was ACF15A, provided by Osaka Gas Co, Japan. All experiments were carried out using the powdered ACF specimen. Scanning electron microscopy indicated that the ACF powdered specimen had a relatively uniform cylindrical shape with a cross-section of approximately 10 µm, retaining the characteristics of the fibrous shape as illustrated in Fig. 1. The acidic functional groups and the basic site on the surface of the ACF specimen were determined using the Boehm method [35]. The acidic functional groups were found to be carboxylic (0.802 mmol/g), lactone (1.07 mmol/g), and phenolic hydroxyl (1.61 mmol/g), whereas the basic sites were 2.07 mmol/g. Although the origin of surface basicity is still under discussion, the pyrone-type structures on the edges of the polyaromatic layers have been suggested as one of the possible basic sites [36]. These surface functional groups could not be detected by solid-state ^{13}C MAS and CPMAS NMR spectra, as they have less concentration than the framework sp^2-carbons of ACF (see ESI). The porosity of ACF15A was characterized using a nitrogen adsorption isotherm obtained at 77 K (see ESI). The micropore volume, surface area, and average slit width were determined via the quenched solid density functional theory (QSDFT) method [37] for the analysis of the nitrogen adsorption isotherm. The resultant micropore volume and surface area were 0.722 cm^3/g and 1475 m^2/g, respectively. The pore size distribution is illustrated in Fig. 2; there are mainly two kinds of micropores, with the average pore width of 1.0 and 1.5 nm. TG/DTA measurement confirmed that the virgin samples of ACF include pre-adsorbed species, such as water, corresponding to approximately 30% of the initial weight of ACF, and pre-adsorbed species are desorbed in the temperature range of 25–80 °C (see ESI).

2.2 Water adsorption measurements

Water adsorption and desorption isotherms were measured at 298 K using an in-house volumetric apparatus. The ACF powdered sample (25.0 mg) was evacuated at 120 °C under a pressure of less than 10^{-5} Pa for 3 h prior to the water adsorption measurements.

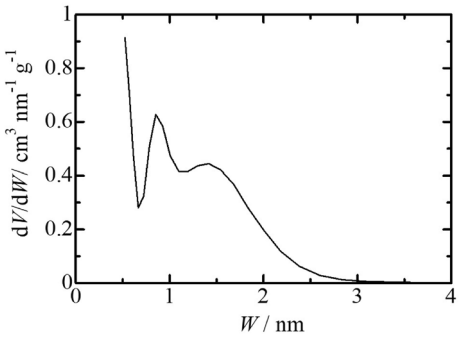

Fig. 2 Pore size distribution determined using the QSDFT analysis for the nitrogen adsorption isotherm of ACF15A. There are two peaks at 1 and 1.5 nm, indicating two kinds of micropores in ACF15A

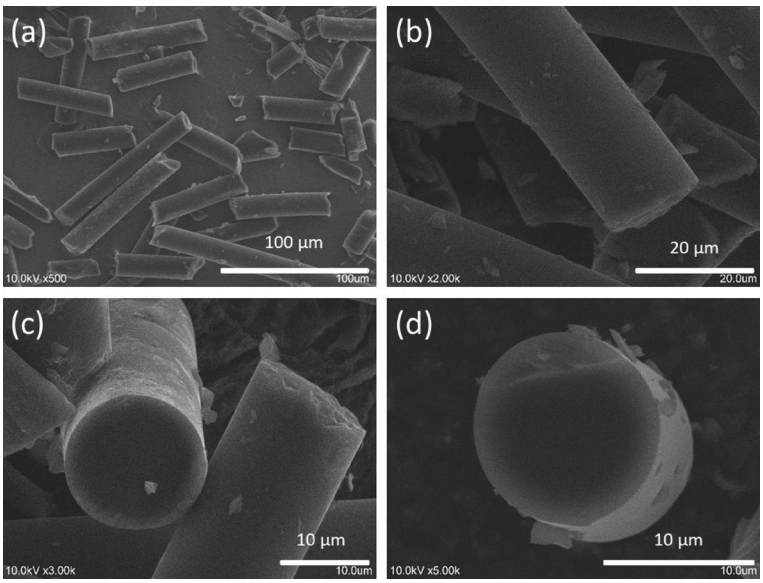

Fig. 1 Scanning electron microscopy (SEM) images of ACF15A powdered specimen. Magnification is as follows: **a** × 500, **b** × 2000, **c** × 3000, and **d** × 5000

2.3 Sample preparation for NMR measurements

ACF was evacuated at 473 K for 3 h prior to the sample preparation. Two methods, vapor adsorption and D_2O drop methods, were used to prepare the NMR measurement samples, as follows. (1) For the vapor adsorption method, a 5 mmø NMR sample tube was used to collect the pretreated ACF specimen. Here, the tube was first vacuum-degassed, and then D_2O vapor was introduced into the sample tube. Samples with varying adsorption amounts were created by adjusting the adsorption time and monitoring the D_2O vapor pressure. Following heavy water adsorption, the tube was sealed with approximately 150 Torr of He gas. (2) For the D_2O drop method, appropriate amounts of ACF powder were collected into the NMR sample tube, and then D_2O was added to achieve the desired pore-filling ratio using a microsyringe. The sample tube was connected to a vacuum line and sealed with approximately 150 Torr of He gas. The sample was annealed at 298 K until equilibrium was reached over a time period of 1–2 d. In methods (1) and (2), the adsorption amounts of D_2O into ACF was measured by weighing the sample before and after adsorption. For a given sample, the pore-filling ratio was determined by calculating the ratio of D_2O adsorbed to the saturated amount of D_2O evaluated from the water adsorption isotherm, based on the weight of the ACF used.

2.4 NMR measurements

NMR measurements were conducted using a JEOL ECA-500 NMR spectrometer (JEOL Ltd., Tokyo, Japan) ($B_0 = 11.75$ T), an Agilent VNS-300 NMR spectrometer (Agilent Technologies, California, USA) ($B_0 = 7.05$ T), and a Bruker AVANCE III spectrometer (Bruker Co., Massachusetts, USA) ($B_0 = 9.40$ T).

The ^2H wide-line NMR spectra were measured using solid-echo pulse sequence on the Bruker AVANCE III spectrometer ($\nu_0 = 61.44$ MHz) at 303 K. The π/2-pulse width was 2.4 μs, and the duration between two π/2-pulses was 30 μs. The echo signal was recorded by delaying 24 μs after the second π/2-pulse. The signal accumulation was 24,000 with 0.5 s of repetition. The ^2H chemical shift was referred to as bulk heavy water (0 ppm).

The spin–lattice relaxation times (T_1) were measured using the inversion recovery method for the temperature range of 298–318 K. The pulse widths of the ^2H nuclei were 22 μs for the JEOL ECA-500 spectrometer and 2.5 μs for the Agilent VNS-300 spectrometer. The repetition time was 4 s. For all examined temperatures, the T_1 values were evaluated with an accuracy of 3%. The T_1 values were measured in the temperature range of 298–320 K to avoid the effect of desorption of adsorbed D_2O. The temperature of the sample was controlled within the accuracy of ± 0.5 K using the temperature controller equipped with the spectrometers.

3 Results and discussion

3.1 Water adsorption isotherm

Figure 3 illustrates the water adsorption and desorption isotherms of ACF15A. The water adsorption isotherm was type V, essentially exhibiting a noticeable uptake near a relative pressure of 0.7 and remarkable hysteresis in the desorption curve [38]. This feature has been typically observed for microporous materials with hydrophobic or slightly hydrophilic surfaces. Prior to the rapid increase of the adsorption branch, the uptake curve was approximately 70 mg g^{-1} (3.9 mmol g^{-1}) of H_2O at a relative pressure of 0.4. This uptake of H_2O is roughly the same as the total amount of the surface functional groups (5.53 mmol g^{-1}). Essentially, at the initial stage of the water adsorption in ACF15A, water molecules adsorbed to the surface functional groups, thus acting as strong adsorption sites. During the next stage, water clusters formed at the strong adsorption sites and grow owing to the strong hydrogen bonding between the water molecules and adsorption sites. At higher relative pressures, the water clusters coalesced and finally water filled the ACF micropores. At a relative pressure of 0.985, water adsorption reached saturation, with the amount of water in ACF15A of 682.4 mg g^{-1}. Using the bulk densities of H_2O (0.997 g cm^{-3}) and D_2O (1.107 g cm^{-3}), this quantity can be converted to the saturated amount of D_2O of 757.7 mg g^{-1}. This value was used for the evaluation of the pore-filling ratio (ϕ) of D_2O in ACF (Fig. 3).

3.2 ^{2}H-NMR spectrum

Figure 4a illustrates a solid-state ^2H-NMR spectrum for a sample with ϕ of 0.55 at 303 K. An extremely sharp

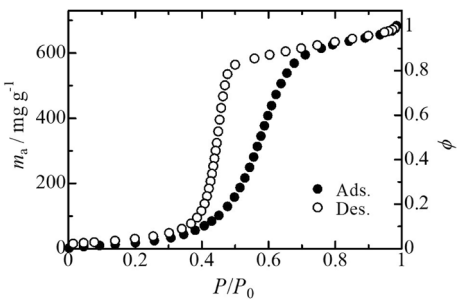

Fig. 3 Water adsorption and desorption isotherms for ACF15A. Both adsorption (●) and desorption (○) branches are shown. The right-hand axis represents the pore-filling ratio of H_2O in the ACF slit-typed micropore

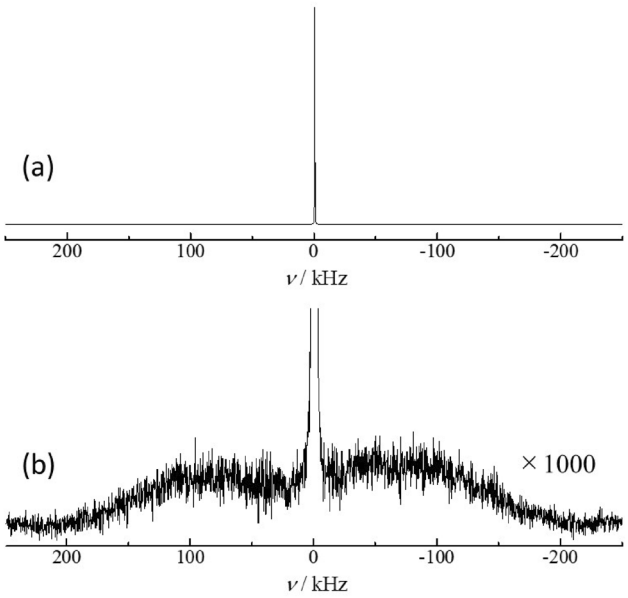

Fig. 4 Solid-state.^{2}H-NMR spectrum for ACF with a D_2O pore-filling ratio of 0.55 at 303 K: overall view (**a**) and enlarged view about a vertical axis (×1000) (**b**)

resonance line was observed near 0 Hz. In addition, a very broad component was observed near the baseline over a range of ± 200 kHz (Fig. 4b). This indicates that the ACF/D_2O sample contains an extremely mobile component and a solid-like, less mobile component. Integrations of these peaks indicate that approximately 89% of the ^{2}H nuclei contribute to the highly mobile narrow component and 11% to the broad component (see ESI). This ratio is close to the mass ratio between adsorbed D_2O and the total amount of surface functional groups in the case of $\phi = 0.55$. The broad component appears to be a line shape similar to the so-called Pake doublet [39–42], in which a peak-to-peak split is ~ 150 kHz. In this case, the ^{2}H quadrupole coupling constant (QCC) is estimated to be approximately 200 kHz. This is a reasonable QCC value for a hydrogen-bonded ^{2}H nucleus in the form of a hydroxyl group and/or carboxylic acid [43]. This suggests that the broad component originates from the ^{2}H nuclei incorporated into the surface functional group by H/D exchange with adsorbed D_2O.

The resonance line for the narrow component had the full linewidth at half maximum of approximately 10–13 ppm. This indicates that the correlation time τ_c of the molecular motion of D_2O in ACF is in the region of extreme narrowing ($\omega_0\tau_c << 1$), indicating that D_2O behaves as a fluid phase. However, the resonance line could not be described by a single Lorentzian function, suggesting that there are multiple components contributing to the narrow resonance line. We successfully achieved satisfactory optimization for the obtained resonance lines using three Lorentzian functions. The results of the optimization for ϕ of 0.55 are shown in Fig. 5a, and those for other pore-filling ratios are also given in ESI.

Figure 5b and c illustrate the ϕ-dependence of the chemical shift values and population of each resonance line. Both the chemical shift values and population of the resonance lines are nearly independent of ϕ. In other words, these components reflect the differences in the intrinsic environment of the ACF micropores, and the exchange among D_2O molecules occupying these environments is considered to be slow compared to the NMR time scale (a few milliseconds).

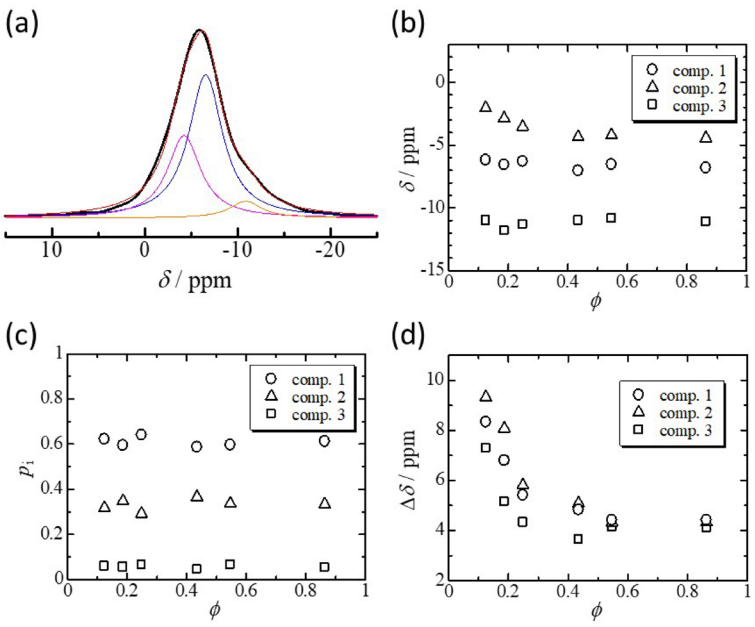

Fig. 5 Result of optimization of the narrow resonance line with $\phi = 0.55$ using the three components of Lorentzian functions (**a**). The resultant parameters are plotted against the D_2O pore-filling ratio: chemical shift (**b**), population (**c**), and line width (**d**)

For the assignment of the resonance lines, the nucleus independent chemical shift (NICS) of the water molecules in carbon slit-shaped micropores, which has been reported by Xing et al., provides a useful reference [29, 44]. They reported that the isotropic NICS, δ_{avg}, averaged over the pore space is related to the pore diameter (atom center-to-center), d, as follows:

$$d = A_{\mathrm{I}}\exp\left(-\delta_{avg}/\delta_{\mathrm{I}}\right) + A_{\mathrm{II}}\exp\left(-\delta_{avg}/\delta_{\mathrm{II}}\right) + d_0 \quad (1)$$

where $\delta_{\mathrm{I}} = -0.53\mathrm{ppm}$, $\delta_{\mathrm{II}} = -3.7\mathrm{ppm}$, $A_{\mathrm{I}} = 16.15\mathrm{nm}$, $A_{\mathrm{II}} = 3.82\mathrm{nm}$, and $d_0 = 0.57\mathrm{nm}$.

The d value represents the pore diameter measured from the center of the carbon atoms comprising the pore wall. Thus, to determine the pore diameter W from the N_2 adsorption isotherm, the diameter of the carbon atoms (0.34 nm) should be subtracted from the evaluated d value. The average values of the chemical shift for each component in Fig. 5b are − 6.57, − 3.57, and − 11.1 ppm for components 1, 2, and 3, respectively. Based on Eq. (1), these shift values can be assigned to the D_2O molecules occupying slit-type micropores with pore diameters of 0.88, 1.7, and 0.42 nm, respectively. The pore sizes estimated from the chemical shifts for components 1 and 2 are in good agreement with the pore size distributions (1 and 1.5 nm) obtained from the N_2 adsorption isotherms, respectively. This suggests that the resonance line for component 1 comes from the D_2O molecules occupying the micropores giving a peak at 1 nm in the pore size distribution and that for component 2 from micropores giving a peak at 1.5 nm. Meanwhile, for component 3, if it is considered to originate from the micropores, the pore size is small (0.42 nm), suggesting that the D_2O molecules may be adsorbed in the micropores that are not detected by N_2 adsorption (but water molecules are accessible). The other possibility is that the water molecules trapped near the pore wall show large negative chemical shifts, which may be attributed to the surface diffusion of D_2O within the pore and on the outer pore surface. In any case, component 3 has a smaller population (< 0.06) than components 1 and 2 (Fig. 5c), and its effect on the T_1 discussion is considered small.

Figure 5d illustrates the D_2O pore-filling ratio dependence of the half-width at half maximum Δδ of the resonance line for each component. The line width decreases significantly up to ϕ of around 0.4 and maintains an almost constant value. The linewidth of the Lorentzian function is related to the effective spin–spin relaxation time (T_2^*) by $\Delta\delta = 1/\pi T_2^*$; an increase in T_2^* indicates a decrease in the correlation time of D_2O molecular motion, τ_c. This suggests that the mobility of the D_2O molecules in the micropore increases significantly in the range of $\phi = 0.1$–0.4. This trend is nearly the same for all three components, suggesting no significant differences in the molecular motion of the D_2O molecules involved in each component. The three components contributing to the narrow resonance line have chemical shift values close to each other, and there is a large overlap between the peaks. Thus, attempting to force the evaluation of T_1 separately for each peak may lead to large errors in the T_1 values. Therefore, in the next section, we will emphasize narrowing the resonance line and discuss the spin-relaxation time (T_1) as a whole, averaged over these three components.

3.3 ^{2}H spin–lattice relaxation time (T_1)

The magnetization recovery curve had two components with different T_1 values for the broadband spectrum (see ESI). We regarded the long T_1 value as the minor component (broad one) because its contribution was less than 1% of that of the short T_1 component. Meanwhile, the magnetization recovery curves decayed exponentially with a single time constant for the narrow resonance lines. This focuses on only the dominant component with the narrow resonance line, which is the primary T_1 component arising from the adsorbed D_2O in the pores.

For the spin–lattice relaxation time (T_1) of D_2O adsorbed in ACF micropores, the ^{2}H-^{2}H and ^{2}H-^{1}H magnetic dipole–dipole interactions and those of ^{2}H nuclear quadrupole are responsible for the relaxation mechanism. The contribution of each interaction to $1/T_1$, which is the relaxation strength, is approximately proportional to the square of the interaction under the conditions of extreme narrowing ($\omega_0\tau_c \ll 1$). The nuclear quadrupole coupling constant ($\chi_Q = 2\pi e^2 Qq/\hbar$), which represents the magnitude of the ^{2}H nuclear quadrupole interaction, is $\chi_Q = 256$ kHz in bulk D_2O (see below). The magnetic dipole interaction is $D_{DD} = \left(\mu_0/4\pi\right)\left(\gamma_D^2\hbar^2/r_{DD}^3\right)$ for ^{2}H-^{2}H and $D_{DH} = \left(\mu_0/4\pi\right)\left(\gamma_D\gamma_H\hbar^2/r_{DH}^3\right)$ for ^{2}H-^{1}H. Assuming that the intramolecular H–H (H–D) distance is $r_{DD} = r_{DH} = 0.158\mathrm{nm}$, $D_{DD} \sim 4.5\mathrm{kHz}$ and $D_{DH} \sim 29\mathrm{kHz}$ are estimated. Thus, the ratio of the relaxation strength due to each interaction is $6.6\times10^{10} : 2.0\times10^{7} : 8.6\times10^{8}$. Since H–D pairs are only produced by the H/D exchange between D_2O and the ACF surface functional groups, the relaxation strength due to the H–D dipole interaction is expected to be further reduced. Therefore, for the D_2O in the ACF pore, the relaxation process dominated by the nuclear quadrupole interaction (T_{1Q}) becomes the main relaxation mechanism; subsequently, the observed relaxation time (T_1) can be approximated to be equal to the relaxation owing to the nuclear quadrupole interaction (T_{1Q}) of D_2O. Thus, the T_1 value can be converted to the rotational correlation time (τ_c) of the D_2O molecules as follows [45].

$$\frac{1}{T_{1Q}} = \frac{3}{8}\chi_Q^2\left(1+\frac{\eta^2}{3}\right)\tau_c, \quad (2)$$

where χ_Q is the nuclear quadrupole coupling constant, and η is the asymmetry parameter of the electric field gradient tensor. The rotational correlation time was determined using the χ_Q and η values for bulk heavy water ($\chi_Q = 256$ kHz and $\eta = 0.164$) [46].

3.3.1 Dependence of T_1 on D_2O pore-filling ratio

Figure 6 illustrates the dependence of ^{2}H T_1 at 303 K on the pore-filling ratio of D_2O. For ϕ below 0.12, T_1 becomes less than 100 ms and is approximately constant. Because the ϕ value is greater than 0.18, T_1 increases and reaches a maximum at ϕ of approximately 0.35. The T_1 value decreases again toward ϕ of 0.4 and then reaches approximately 170 ms. Subsequently, it gradually increases after ϕ of 0.43. This suggests that the mobility of D_2O molecules within the ACF micropores changes with ϕ.

The ϕ-dependence of τ_c is also shown in Fig. 6. In the regions where $\phi < 0.12$, τ_c has values more than 11 ps. This value is five times higher than that for bulk water ($\tau_c = 2.0$ ps). The high value of τ_c is attributed to the suppression of the rotational motion of the D_2O molecules, which is caused by the formation of strong hydrogen bonds between the D_2O molecules and the surface functional groups that act as strong hydrogen acceptors or donors. The τ_c value is consistent with ϕ of 0.14 necessary for the adsorbed D_2O molecules to interact with all of the surface functional groups (see ESI). Therefore, the τ_c values for ϕ in the range of 0.19–0.44 are considered to reflect the intermolecular structure of the adsorbed D_2O molecules. Essentially, the growth of the water clusters is followed by the formation of a continuous fluid phase in the ACF micropores. This is consistent with the scheme of the detailed nucleation and growth processes of water inside activated carbon micropores revealed by the nucleus-independent chemical shift (NICS) of water in a previous study [30]. In Sect. 3.5, we quantitatively analyze the dependence of τ_c on ϕ based on the chemical exchange effect.

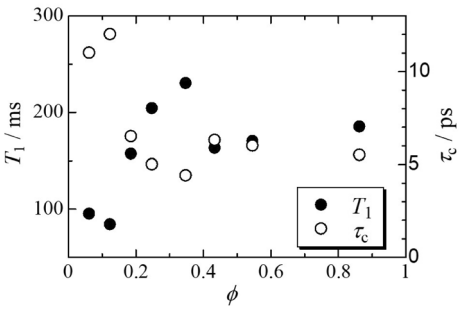

Fig. 6 Pore-filling ratio (ϕ) dependence of the ^{2}H spin–lattice relaxation time (T_1) and the correlation time (τ_c) of D_2O reorientation at 303 K. The error bars are within the data symbols. The T_1 and τ_c values clearly depend on ϕ, suggesting that the local structure of D_2O confined in ACF critically affects the reorientation of D_2O molecules

3.3.2 Temperature dependence of ^{2}H T_1

The intermolecular interactions between a D_2O molecule and the adsorption sites in the ACF micropore can also be examined through the evaluation of the Arrhenius activation energy (E_a), which is determined from the temperature dependence of τ_c. Figure 7 shows the Arrhenius plot of τ_c. All of the specimens follow Arrhenius's law, thus suggesting that the temperature-dependent behavior of τ_c is controlled by the thermal activation process ($\tau_c = \tau_0 \exp[E_a/RT]$). The obtained activation energies are listed in Table 1.

At the low pore-filling ratio ($\phi < 0.12$), the reorientation of D_2O molecules is suppressed by the strong hydrogen bonding to the surface functional groups. According to the EJM (see below) that explains the microscopic process of D_2O molecular reorientation, the energy barrier is dominated primarily by two factors [34], namely framework fluctuations that cause the hydrogen-bonded D_2O pairs to flip

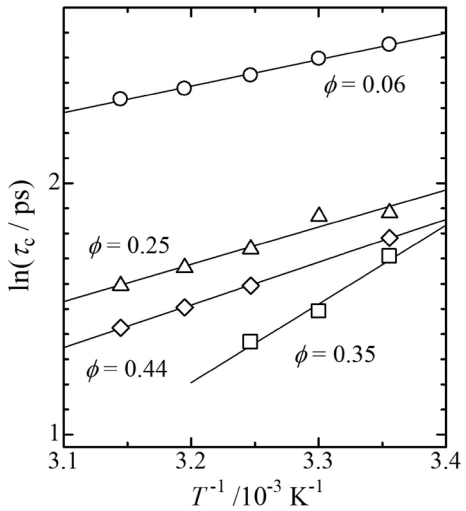

Fig. 7 Arrhenius plot of the correlation times for the D_2O reorientation

Table 1 Activation parameters determined from the Arrhenius plots of τ_c

ϕ	E_a (kJ mol^{-1})	τ_0 (s)
0.06	8.8 (±0.1)	(3.7 ± 0.1) × 10^{-13}
0.25	12 (±1)	(4.7 ± 0.1) × 10^{-14}
0.35	27(±4)	(2 ± 1) × 10^{-16}
0.44	14 (±1)	(2.0 ± 0.1) × 10^{-14}

together, and the proximity of a second D_2O molecule to the hydrogen bond site. However, because the functional groups attached to the micropore surface cannot flip together with a D_2O molecule, the effect of the framework fluctuations on the activation energy is believed to be minimal. In the vicinity of the pore surface, the strong potential field of the micropores effectively interacts with the adsorbed molecules. This is expected to reduce the thermal fluctuations through a pseudo-low-temperature effect. Therefore, the area surrounding the D_2O molecules that are trapped by the surface functional groups can be accessed by overcoming a relatively low energy barrier (8.8 kJ/mol).

As the pore-filling ratio increases and the number of the D_2O molecules in the micropore exceeds that of the surface functional groups ($\phi = 0.14$) (see ESI), D_2O molecules that exhibit significantly weaker interactions with the surface functional groups appear. These molecules can move within the micropore while exchanging hydrogen bonds with the D_2O clusters formed around the surface functional groups. These D_2O molecules also act as hydrogen acceptors during the hydrogen bond exchange reaction. These D_2O molecules require energy to break the hydrogen bonds with the D_2O cluster and move around in the micropore, thus contributing to the activation energy for the reorientation motion and leading to an activation energy of 12 kJ/mol. Furthermore, when the ϕ value exceeds 0.3, the D_2O molecules moving in the pores also form hydrogen bonds, thus leading to the growth of the water clusters, resulting in the formation of a hydrogen-bond network and increasing the number of hydrogen bonds per D_2O molecule. Consequently, this increases the activation energy to 26 kJ/mol. However, when the ϕ value reaches 0.44, the density of the D_2O molecules in the micropore approaches that of bulk D_2O. At this point, the hydrogen-bond network becomes almost complete, resulting in a reduction in the contribution of translational motion. The local structural fluctuations of the D_2O molecules allow for hydrogen bond exchange and associated reorientation. Consequently, the activation energy is almost the same as that of bulk D_2O, which is 14.6 kJ/mol [34].

3.4 Delay effect of reorientation motion

The EJM has been used to describe the reorientation of water molecules [33, 34]. This model treats the local fluctuations of hydrogen-bonded water molecules and considers the contributions of both the changes in the direction of water molecules by jumping (jump process) and the collective flipping of a pair of water molecules linked by a hydrogen bond (framework flipping process). The reorientation rate ($1/\tau_{reor}^{EMJ}$) of the water molecule is given by the sum of both the rate of the jump process (τ_{jump}) and the rate of the framework flipping process (τ_{frame}), according to $1/(\tau_{reor}^{EMJ}) = 1/\tau_{reor} + 1/\tau_{frame}$. Molecular dynamics simulations using the SPC/E molecular force field for water yield $\tau_{reor}^{EJM} = 2.2$ ps, $\tau_{reor} = 3.6$ ps, and $\tau_{frame} = 5.6$ ps at 300 K [34]. Thus, the reorientation of water molecules is dominated by the faster jump process.

When applying this model to the D_2O confined in the ACF slit-shaped micropores, two contributions are considered to affect the jump time of the D_2O molecules [47]: 1) the nanoconfinement effect (reduction of free volume around D_2O) and 2) the effect of the surface functional groups (capture of D_2O molecules through hydrogen bonding). For the hydrogen-bond exchange reaction, these effects can be accounted for by the transition-state excluded volume (TSEV), and the transition-state hydrogen bonding (TSHB) factor.

The TSEV effect slows the delay of the molecular motion of D_2O. The delay factor of the molecular motion due to TSEV is denoted as ρ_V and is given by the ratio of the jump time of the water molecules in the slit-shaped micropores to that of bulk water [47, 48]:

$$\rho_V = \tau_{jump}^{pore}/\tau_{jump}^{bulk} = \frac{f}{1-f} \tag{3}$$

where "f" is the fraction of the space that is unavailable for the transition state of the hydrogen-bonding exchange reactions. This corresponds to the fraction of the circular ring surrounding the O–H…O hydrogen bond that is geometrically overlapped by the pore walls and surface functional groups. For bulk water, this fraction is determined by the intermolecular distance between the hydrogen-bonded water molecules and the angle of the jump of the hydrogen atom. For spatially extended hydrophobic surfaces, the f value of approximately 1/2 ($\rho_V = 1.8$) has been reported [49]. For ϕ of 0.35, the ρ_V value is estimated to be 2.2 (i.e., 4.4 ps/2.0 ps) at 303 K, which is in good agreement with the reported value. Thus, the confinement in the ACF nanopores delays the reorientational motion of the D_2O molecules at ϕ of 0.35 through the TSEV effect in the hydrogen-bond exchange reaction. As the ϕ value increases to approximately 0.44, the τ_c and ρ_V values reach 6.3 ps and 3.2, respectively. This suggests that the filling of D_2O into the ACF micropores increases the TSEV effect owing to the restricted space between the D_2O molecules.

The TSHB factor accounts for the asymmetry in the strength of the hydrogen bonding between the water molecules and other hydrogen bonding acceptors. The TSHB factor is the difference between the transition Gibbs energies of hydrogen bonding at the non-water hydrogen-bond acceptor sites ($\Delta G^{\ddagger}_{A}$) and hydrogen bonding for bulk water ($\Delta G^{\ddagger}_{bulk}$) and is denoted by $\Delta\Delta G^{\ddagger}$. This factor specifies whether the hydrogen bond exchange reaction is accelerated or retarded compared to that in bulk water. Thus, the TSHB factor ρ_{HB} is expressed as $\rho_{HB} = \exp(\Delta\Delta G^{\ddagger}/kT)$ [47, 48]. When both

the effects of steric hindrance and hydrogen bonding in the nanospace are considered, the jump time of a water molecule is given by $\tau_{jump} = \rho_V \cdot \rho_{HB} \cdot \tau_{jump}^{bulk}$ [47]. For relatively strong hydrogen bonding acceptors, such as carboxyl and amino groups, ρ_{HB} is known to have values between 2 and 4 [50], thus indicating a significant delayed effect on the jump time of water molecules. The ACF micropore walls also contain strong hydrogen bonding acceptor sites, such as carboxyl and lactone groups, and basic sites. These are expected to form strong hydrogen bonds with the adsorbed D_2O molecules and suppress their reorientation. At ϕ of 0.06, $\tau_c = 11.0$ ps at 303 K; then, the ρ_{HB} value is estimated as 2.5 by assuming $\tau_{jump}^{bulk} = 2.0$ ps and $\rho_V = 2.2$. These results are consistent with the previously reported values [50]. Therefore, the rotational motion of D_2O at ϕ below 0.12 is delayed primarily by the formation of strong hydrogen bonds with surface functional groups.

Furthermore, the activation energy (E_a) provides insight into the hydrogen bonding of the D_2O molecules in the ACF15A micropores. For bulk D_2O, reportedly, the E_a value is 11.7 kJ/mol per hydrogen bond [51]. Assuming that the hydrogen bonds between the D_2O molecules in the ACF15A micropore have a similar bond energy to the molecules in the bulk, the E_a value of 26 kJ/mol at a ϕ of 0.35 is equivalent to the energy required to break 2.3 hydrogen bonds during the rotational motion of D_2O molecules. Essentially, the number of hydrogen bonds formed by a D_2O molecule in the ACF15A micropore is approximately 60% of that in hexagonal ice (4), and 70% of that in bulk H_2O (3.4 on average) [52]. Thus, the adsorbed D_2O in the ACF15A micropores has a much sparser hydrogen bonding network.

3.5 Effects of the chemical exchange of D_2O molecules

The D_2O molecules adsorbed in the ACF micropores are found at the adsorption sites near the pore surface (S) containing surface functional groups and in the spaces away from the pore surface (W). Although the W site also has a strong adsorption potential field enhanced by the micropores, the S site can adsorb D_2O molecules more strongly than the W sites because of the strong hydrogen-bonding interactions with the surface functional groups and the formation of the image-potential states in graphene. The D_2O molecules adsorbed in the ACF micropores exchange dynamically between both sites, as denoted by $S \rightleftharpoons W$. Applying the EJM to the D_2O molecules in the micropores, the average reorientation time $\left\langle \tau_{reor}^{EJM} \right\rangle$ can be represented using the reorientation times τ_{reor}^{S} and τ_{reor}^{W} and the site populations p^S and p^W of the two sites [53, 54] as $p^S\tau_{reor}^{S} + p^W\tau_{reor}^{W}$. The reorientation time at the W site, τ_{reor}^{W}, is given by the average of the correlation time for the reorientation involving deuteron transfer from the W site to the S site, τ_{reor}^{WS}, and time τ_{reor}^{WW} for the reorientation involving deuteron transfer between W sites, as follows.

$$\frac{1}{\tau_{reor}^{W}} \approx \frac{1 - p^{S\to W}}{\tau_{reor}^{WS}} + \frac{p^{S\to W}}{\tau_{reor}^{WW}} \tag{4}$$

where $p^{S\to W}$ is the probability of the D_2O molecule that initially occupies the S site to jump to the W site. By expressing $\left\langle \tau_{reor}^{EJM} \right\rangle$ as a function of the pore-filling ratio, we can qualitatively analyze the pore-filling ratio dependence of τ_c. First, we approximate τ_{reor}^{S} and τ_{reor}^{WW} based on the τ_c values obtained at the low pore-filling ratio ($\phi < 0.12$) and high pore-filling ratio ($\phi > 0.55$), respectively. The τ_{reor}^{WS} is shorter than τ_{reor}^{S} and τ_{reor}^{WW} because the D_2O molecule re-orients rapidly when fast deuteron transfer to the strong hydrogen bond acceptor sites occurs. Next, the τ_{reor}^{WS} value is approximated to be similar to or shorter than τ_c for bulk D_2O. Furthermore, the water adsorption process in 2D hydrophobic space is characterized by forming water clusters, followed by their growth and coalescence, resulting in effective water adsorption. This process also increases the probability of migration of the D_2O molecules (or D atoms), as described by the 2D percolation theory. Essentially, $p^{S\to W}$ can be approximated by the following sigmoidal function [55].

$$p^{S\to W} = \frac{1}{2}\left[1 + \tanh\left(\frac{\phi - \phi_c}{L}\right)\right] \tag{5}$$

where ϕ_c is the critical pore-filling ratio, which is 1/2 in 2D bond percolation and 0.592746 in 2D site percolation [55]. The value of "L" is a variable parameter and depends on the size of the system. For $\phi < 0.14$, the populations of the S and W sites are $p^S = 1$ and $p^W = 0$, whereas, for $\phi > 0.15$, the population of each site depends on the site stability and can be represented by the Boltzmann-like distribution, as follows.

$$p^S = \phi \exp\left[-b(\phi - \phi_0)\right] \tag{6}$$

$$p^W = 1 - p^S \tag{7}$$

where b is a constant determining the shape of the distribution. Using these relationships, we were able to qualitatively reproduce the dependence of τ_c on ϕ, as shown in Fig. 8, thereby obtaining the following parameters; $\phi_c = 0.3$, $\tau_{reor}^{WS} = 0.5$ ps, $\tau_{reor}^{WW} = 5.5$ ps, $\tau_{reor}^{S} = 11.5$ ps, $\phi_0 = 0.15$, $b = 2$, and $L = 0.05$. The b value obtained at 303 K corresponds to the energy difference of approximately 78 meV between the S site and the W site. Thus, the dependence of the D_2O rotational motion in the ACF micropores on ϕ can be explained by the effect of the chemical exchange between the adsorption sites near the pore surface (S) and the D_2O molecules in the space away from the pore surface (W). In

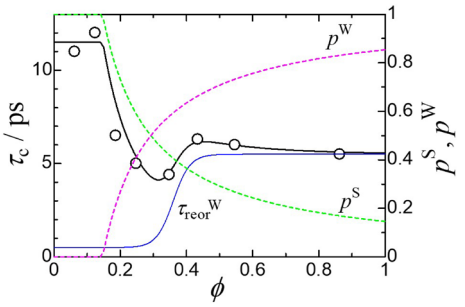

Fig. 8 Pore-filling ratio dependence of τ_c at 303 K. The exchange model reproduces well the experimental data described by the solid curve (black line). The populations of the S and W sites are shown by dashed lines (light-green for p^S and pink for p^W). The reorientation time ($\tau_{reor}{}^W$; blue solid line) of D_2O occupying the W site suddenly increases at ϕ of approximately 0.35 owing to the site-percolation linkages of the water clusters (Color figure online)

particular, we can conclude that the minimal rotational correlation time observed at a ϕ of 0.3 is caused by the crossover between the D_2O molecules moving freely within the micropore and the development of a hydrogen bonding network due to the growth of the water clusters as well as the site-percolation linkages of the water clusters.

4 Conclusion

The reorientational motion of the D_2O molecules adsorbed in ACF was investigated using ^{2}H-NMR. The ^{2}H-NMR spectrum at the ambient temperature showed an extremely sharp resonance line that was well-described by the three kinds of Lorentzian-type functions, with a full-width at the half maximum of approximately 3–9 ppm. This indicates that D_2O in ACF behaves as a fluid phase. According to the nucleus independent chemical shift (NICS) of the water molecules in carbon slit-shaped micropores, these three components were assigned to the D_2O molecules confined in the ACF micropores with different pore sizes (1, 1.5, and < 0.42 nm).

The pore-filling ratio and temperature dependence of the ^{2}H spin–lattice relaxation time (T_1) were further examined based on the measurements of the water adsorption isotherm of ACF, revealing the dynamics of the D_2O molecules in the D_2O adsorption mechanism. The observed T_1 values were converted to the rotational correlation times (τ_c) of the D_2O molecules. The obtained τ_c values showed a remarkable dependence on ϕ and temperature, indicating that the reorientation of the D_2O molecule in ACF is significantly affected by the adsorption of D_2O into ACF that consists of hydrogen bonding with the surface functional group, water cluster formation, and growth of the hydrogen bonding network. For ϕ below 0.12, the slow reorientation of D_2O was dominated by the formation of strong hydrogen bonds between the D_2O molecules and the surface functional groups acting as strong hydrogen acceptors or donors. For ϕ ranging from 0.19 to 0.44, the τ_c values reflected the structural change from water clusters to the continuous fluid phase in the ACF micropores.

The EJM can explain the reorientational correlation time of the D_2O molecules confined in the slit-shaped micropores of ACF as arising predominantly from two contributions: the TSEV effect and the TSHB factor. These effects delayed the reorientational motion of D_2O molecules through the reduction of the free volume around D_2O due to nanoconfinement and the effect of the hydrogen bonding of D_2O with the surface functional groups.

The ϕ-dependence of τ_c was explained by the effect of the chemical exchange between the adsorption sites near the pore surface and the central space of the pore away from the pore surface. The minimum of τ_c at a ϕ of approximately 0.3 was considered to be due to the crossover between the D_2O molecules moving freely within the micropore and the development of a hydrogen-bonding network through the growth of water clusters as well as their site-percolation linkages.

Thus, this study examined the molecular motion of D_2O confined in ACF using ^{2}H T_1, characterized the dynamics of the adsorbed D_2O molecules, and revealed the adsorption mechanism of D_2O into the ACF micropores from the viewpoint of the D_2O molecular motion. We believe that these findings open a new avenue for the development of a molecular theory of water adsorption in hydrophobic sub-nanoscale spaces. For example, the NMR technique used in this study, which monitors the molecular motion of water as a molecular probe, may make it possible to examine the specific adsorption behavior of water observed in graphene and graphene oxide, which has recently attracted significant attention.

Supplementary Information The online version contains supplementary material available at https://doi.org/10.1007/s10450-023-00433-8.

Acknowledgements The authors thank Dr. Naoya Inazumi and Dr. Yasuto Todokoro of the Analytical Instrument Facility, Graduate School of Science, Osaka University for their constructive advice and guidance concerning solid-state NMR measurements.

Author contributions TU conceived the study design, analyzed the experimental data, discussed the results, and wrote the manuscript. TA performed the NMR measurements and wrote the experimental section of the manuscript. RI and IT performed the adsorption isotherm measurements and constructed the adsorption isotherms. TU and IT reviewed the manuscript.

Funding Open Access funding provided by Osaka University. This research was supported by a JSPS KAKENHI Grant-in-Aid for Scientific Research (C) (Grant Number JP21K04979). This work was also the result of using research equipment shared in the Ministry of Education, Science Sports and Culture and the Science and Technology Agency (MEXT) project for promoting the public utilisation of advanced

research infrastructure (Program for supporting construction of core facilities) Grant Number JPMXS0441200021 and JPMXS0441200023.

Data availability The data presented in this article will be available from the corresponding author on reasonable request.

Declarations

Conflict of interest The authors have no relevant financial or non-financial interests to disclose.

Ethical approval Not applicable.

References

1. Chaplin, M.F.: Structure and properties of water in its various states, Encyclopedia of water: science, technology, and society. In: Maurice, P.A. (ed.). Wiley (2019)
2. Dunaeva, A.N., Antsyshkin, D.V., Kuskov, O.L.: Phase diagram of H_2O: thermodynamic functions of the phase transitions of high-pressure ices. Sol. Syst. Res. **44**, 202–222 (2010)
3. Krüger, Y., Mercury, L., Canizarès, A., Marti, D., Simon, P.: Metastable phase equilibria in the ice II stability field: a Raman study of synthetic high-density water inclusions in quartz. Phys. Chem. Chem. Phys. **21**, 19554–19566 (2019)
4. Yamane, R., Komatsu, K., Gouchi, J., Uwatoko, Y., Machida, S., Hattori, T., Ito, H., Kagi, H.: Experimental evidence for the existence of a second partially-ordered phase of ice VI. Nat. Commun. **12**, 1129 (2021)
5. Gasser, T.M., Thoeny, A.V., Fortes, A.D., Loerting, T.: Structural characterization of ice XIX as the second polymorph related to ice VI. Nat. Commun. **12**, 1128 (2021)
6. Millot, M., Hamel, S., Rygg, J.R., Celliers, P.M., Collins, G.W., Coppari, F., Fratanduono, D.E., Jeanloz, R., Swift, D.C., Eggert, J.H.: Experimental evidence for superionic water ice using shock compression. Nat. Phys. **14**, 297–302 (2018)
7. Hansen, T.C.: The everlasting hunt for new ice phases. Nat. Commun. **12**, 3161 (2021)
8. Salzmann, C.G., Loveday, J.S., Rosu-Finsen, A., Bull, C.L.: Structure and nature of ice XIX. Nat. Commun. **12**, 3162 (2021)
9. Kapil, V., Schran, C., Zen, A., Chen, J., Pickard, C.J., Michaelides, A.: The first-principles phase diagram of monolayer nanoconfined water. Nature **609**, 512–516 (2022)
10. Takaiwa, D., Hatano, I., Koga, K., Tanaka, H.: Phase diagram of water in carbon nanotubes. Proc. Natl. Acad. Sci. U.S.A. **105**, 39–43 (2008)
11. Sugahara, A., Ando, Y., Kajiyama, S., Yazawa, K., Gotoh, K., Otani, M., Okubo, M., Yamada, A.: Negative dielectric constant of water confined in nanosheets. Nat. Commun. **10**, 850 (2019)
12. Otake, K.I., Otsubo, K., Komatsu, T., Dekura, S., Taylor, J.M., Ikeda, R., Sugimoto, K., Fujiwara, A., Chou, C.P., Sakti, A.W., Nishimura, Y., Nakai, H., Kitagawa, H.: Confined water-mediated high proton conduction in hydrophobic channel of a synthetic nanotube. Nat. Commun. **11**, 843 (2020)
13. Singh, G., Lee, J.M., Kothandam, G., Palanisami, T., Al-Muhtaseb, A.H., Karakoti, A., Yi, J., Bolan, N., Vinu, A.: A review on the synthesis and applications of nanoporous carbons for the removal of complex chemical contaminants. Bull. Chem. Soc. Jpn **94**, 1232–1257 (2021)
14. Daley, M.A., Tandon, D., Economy, J., Hippo, E.J.: Elucidating the porous structure of activated carbon fibers using direct and indirect methods. Carbon **34**, 1191–1200 (1996)
15. Kaneko, K., Ishii, C., Ruike, M., Kuwabara, H.: Origin of super-high surface area and microcrystalline graphitic structures of activated carbons. Carbon **30**, 1075–1088 (1992)
16. Kimura, T., Kanoh, H., Kanda, T., Ohkubo, T., Hattori, Y., Higaonna, Y., Denoyel, R., Kaneko, K.: Cluster-associated filling of water in hydrophobic carbon micropores. J. Phys. Chem. B **108**, 14043–14048 (2004)
17. Ohba, T., Kaneko, K.: Cluster-associated filling of water molecules in slit-shaped graphitic nanopores. Mol. Phys. **105**, 139–145 (2007)
18. Ohba, T., Kanoh, H., Kaneko, K.: Cluster-growth-induced water adsorption in hydrophobic carbon nanopores. J. Phys. Chem. B **108**, 14964–14969 (2004)
19. Horikawa, T., Yuasa, R., Yoshida, Do, K., Do, D.D.: Temperature dependence of water cluster on functionalized graphite. Carbon **183**, 380–389 (2021)
20. Liu, L., Zeng, W., Tan, S.J., Liu, M., Do, D.D.: Microscopic insights into water adsorption in carbon nanopores—the role of acidic and basic functional groups and their configurations. Phys. Chem. Chem. Phys. **23**, 18369–18377 (2021)
21. Ito, H., Iiyama, T., Ozeki, S.: Kinetics of cluster-mediated filling of water molecules into carbon micropores. J. Phys. Chem. C **119**, 4118–4125 (2015)
22. Ito, H., Vallejos-Burgos, F., Ono, Y., Yoshimoto, M., Kaneko, K., Futamura, R., Iiyama, T., Matsumoto, A.: Isotope effect on adsorption diffusivity of water molecules in hydrophobic carbon micropores. Carbon **168**, 415–418 (2020)
23. Liu, L., Tan, S.J., Horikawa, T., Do, D.D., Nicholson, D., Liu, J.: Water adsorption on carbon—a review. Adv. Colloid Interface Sci. **250**, 64–78 (2017)
24. Futamura, R., Iiyama, T., Hamasaki, A., Ozeki, S.: Negative thermal expansion of water in hydrophobic nanospaces. Phys. Chem. Chem. Phys. **14**, 981–986 (2012)
25. Iiyama, T., Fujisaki, F., Futamura, R., Hamasaki, A., Ozeki, S., Hoshikawa, A., Ishigaki, T.: Structure determination of hydrogen-bonding network of water in hydrophobic nanospace by neutron and X-ray diffractions. Chem. Lett. **41**, 1267–1269 (2012)
26. Sugiyama, Y., Futamura, R., Iiyama, T.: Ice-like structure of water confined in hydrophobic sub-nanometer spaces at room temperature. Chem. Lett. **51**, 760–764 (2022)
27. Jiao, S., Xu, Z.: Non-continuum intercalated water diffusion explains fast permeation through graphene oxide membranes. ACS Nano **11**, 11152–11161 (2017)
28. Omichi, H., Ueda, T., Miyakubo, K., Eguchi, T.: Solid-state ^2H NMR study of nanocrystal formation of D_2O and their dynamic aspects in ACF hydrophobic nanospaces. Chem. Lett. **36**, 256–257 (2007)
29. Wang, H.J., Kleinhammes, A., McNicholas, T.P., Liu, J., Wu, Y.: Water adsorption in nanoporous carbon characterized by in situ NMR: Measurements of pore size and pore size distribution. J. Phys. Chem. C **118**, 8474–8480 (2014)
30. Song, Y., Chong, Y., Raghavan, A., Xing, Y., Ling, Y., Kleinhammes, A., Wu, Y.: Nucleation and growth process of water

adsorption in micropores of activated carbon revealed by NMR. J. Phys. Chem. C **121**, 8504–8509 (2017)
31. Vittadini, E., Dickinson, L.C., Lavoie, J.P., Pham, X., Chinachoti, P.: Water mobility in multicomponent model media as studied by ^{2}H and ^{17}O NMR. J. Agric. Food Chem. **51**, 1647–1652 (2003)
32. Ropp, J., Lawrence, C., Farrar, T.C., Skinner, J.L.: Rotational motion in liquid water is anisotropic: a nuclear magnetic resonance and molecular dynamics simulation study. J. Am. Chem. Soc. **123**, 8047–8052 (2001)
33. Laage, D., Hynes, J.T.: A molecular jump mechanism of water reorientation. Science **311**, 832–835 (2006)
34. Laage, D., Hynes, J.T.: On the molecular mechanism of water reorientation. J. Phys. Chem. B **112**, 14230–14242 (2008)
35. Boehm, H.P.: Some aspects of the surface chemistry of carbon blacks and other carbons. Carbon **32**, 759–769 (1994)
36. Boehm, H.P.: Surface oxides on carbon and their analysis: a critical assessment. Carbon **40**, 145–149 (2002)
37. Ravikovitch, P.I., Neimark, A.V.: Density functional theory model of adsorption on amorphous and microporous silica materials. Langmuir **22**, 11171–11179 (2006)
38. Thommes, M., Kaneko, K., Neimark, A.V., Olivier, J.P., Rodriguez-Reinoso, F., Rouquerol, J., Sing, K.S.W.: Physisorption of gases, with special reference to the evaluation of surface area and pore size distribution (IUPAC Technical Report). Pure Appl. Chem. **87**, 1051–1069 (2015)
39. Gladden, L.F., Sousa-Gonçalves, J.A., Alexander, P.: Adsorption and transport of ethane and ethene in zeolite NaA: ^{2}H NMR and Monte Carlo lattice dynamics studies. J. Phys. Chem. B **101**, 10121–10127 (1997)
40. Kolokolov, D.I., Arzumanov, S.S., Stepanov, A.G., Jobic, H.: Dynamics of linear n-C_6−n-C_{22} alkanes inside 5A zeolite studied by ^{2}H NMR. J. Phys. Chem. C **111**, 4393–4403 (2007)
41. Kolokolov, D.I., Glaznev, I.S., Aristov, Y.I., Stepanov, A.G., Jobic, H.: Water dynamics in bulk and dispersed in silica $CaCl_2$ hydrates studied by ^{2}H NMR. J. Phys. Chem. C **112**, 12853–12860 (2008)
42. Kolokolov, D.I., Kazantsev, M.S., Luzgin, M.V., Jobic, H., Stepanov, A.G.: Characterization and dynamics of the different protonic species in hydrated 12-tungstophosphoric acid studied by ^{2}H NMR. J. Phys. Chem. C **118**, 30023–30033 (2014)
43. Hunger, M., Horvath, T.: Adsorption of methanol on brønsted acid sites in zeolite H-ZSM-5 investigated by multinuclear solid-state NMR spectroscopy. J. Am. Chem. Soc. **118**, 12302–12308 (1996)
44. Xing, Y.Z., Luo, Z.X., Kleinhammes, A., Wu, Y.: Probing carbon micropore size distribution by nucleus independent chemical shift. Carbon **77**, 1132–1139 (2014)
45. Fung, B.M., McGaughy, T.W.: Study of spin-lattice and spin-spin relaxation times of ^{1}H, ^{2}H, and ^{17}O in muscular water. Biophys. J. **28**, 293–303 (1979)
46. Ludwig, R., Weinhold, F., Farrar, T.C.: Experimental and theoretical determination of the temperature dependence of deuteron and oxygen quadrupole coupling constants of liquid water. J. Chem. Phys. **103**, 6941–6950 (1995)
47. Laage, D., Stirnemann, G., Sterpone, F., Rey, R., Hynes, J.T.: Reorientation and allied dynamics in water and aqueous solutions. Annu. Rev. Phys. Chem. **62**, 395–416 (2011)
48. Laage, D., Stirnemann, G., Hynes, J.T.: Why water reorientation slows without iceberg formation around hydrophobic solutes. J. Phys. Chem. B **113**, 2428–2435 (2009)
49. Stirnemann, G., Rossky, P.J., Hynes, J.T., Laage, D.: Water reorientation, hydrogen-bond dynamics and 2D-IR spectroscopy next to an extended hydrophobic surface. Faraday Discuss. **146**, 263–281 (2010)
50. Sterpone, F., Stirnemann, G., Hynes, J.T., Laage, D.: Water hydrogen-bond dynamics around amino acids: the key role of hydrophilic hydrogen-bond acceptor groups. J. Phys. Chem. B **114**, 2083–2089 (2010)
51. Walrafen, G.E., Yang, W.H., Chu, Y.C., Hokmabadi, M.S.: Raman OD-stretching overtone spectra from liquid D_2O between 22 and 152 °C. J. Phys. Chem. **100**, 1381–1391 (1996)
52. Pethes, I., Pusztai, L., Ohara, K., Kohara, S., Darpentigny, J., Temleitner, L.: Temperature-dependent structure of methanol-water mixtures on cooling: X-ray and neutron diffraction and molecular dynamics simulations. J. Mol. Liq. **314**, 113664 (2020)
53. Laage, D., Hynes, J.T.: Reorientional dynamics of water molecules in anionic hydration shells. Proc. Natl. Acad. Sci. U.S.A. **104**, 11167–11172 (2007)
54. Stirnemann, G., Wernersson, E., Jungwirth, P., Laage, D.: Mechanisms of acceleration and retardation of water dynamics by ions. J. Am. Chem. Soc. **135**, 11824–11831 (2013)
55. Sotta, P., Long, D.: The crossover from 2D to 3D percolation: theory and numerical simulations. Eur. Phys. J. E Soft Matter **11**, 375–387 (2003)